How skilful are nowcasting satellite applications facility products for tropical Africa?

Hill, P. G. ORCID: https://orcid.org/0000-0002-9745-2120, Stein, T. H. M. ORCID: https://orcid.org/0000-0002-9215-5397, Roberts, A. J., Fletcher, J. K., Marsham, J. H. and Groves, J. (2020) How skilful are nowcasting satellite applications facility products for tropical Africa? Meteorological Applications, 27 (6). e1966. ISSN 1350-4827 doi: 10.1002/met.1966 Available at https://centaur.reading.ac.uk/93934/

Received: 22 May 2020 | Revised: 24 September 2020 | Accepted: 14 October 2020

DOI: 10.1002/met.1966

RESEARCH ARTICLE

Meteorological Applications
Science and Technology for Weather and Climate
Open Access
RMetS

How skilful are Nowcasting Satellite Applications Facility products for tropical Africa?

Peter G. Hill[1] | **Thorwald H.M. Stein**[1] | **Alexander J. Roberts**[2,3] | **Jennifer K. Fletcher**[2,3] | **John H. Marsham**[2,3] | **James Groves**[3]

[1]Department of Meteorology, University of Reading, Reading, UK

[2]School of Earth and Environment, University of Leeds, Leeds, UK

[3]National Centre for Atmospheric Science, Leeds, UK

Correspondence
Peter G. Hill, Department of Meteorology, University of Reading, Reading, RG6 6BB, UK.
Email: p.g.hill@reading.ac.uk

Funding information
Global Challenges Research Fund, African SWIFT programm, Grant/Award Numbers: NE/P021077/1, NE/r000034/1

Abstract

Satellite nowcasting potentially provides a vital opportunity to mitigate against the risks of severe weather in tropical Africa, where population growth and climate change are exposing an ever growing number of people to weather hazards. Numerical weather prediction demonstrates limited skill for much of Africa and weather radars are rare. However, geostationary satellites provide excellent spatial and temporal coverage of the often long-lasting convective storms that deliver heavy rain, lightning and strong winds, presenting a valuable opportunity for satellite nowcasting. Here, we evaluate the skill of satellite nowcasting products for tropical Africa: these products are routinely generated, but to our best knowledge never routinely used in tropical Africa before the Global Challenges Research Fund African SWIFT (Science for Weather Information and Forecasting Techniques) project. Focusing in particular on convective rainfall rate (CRR) and rapidly developing thunderstorm convection warning (RDT-CW) products, we demonstrate that both are useful nowcasting tools. The CRR product produces very different rainfall climatologies for day and night in tropical Africa. This is associated with greater skill of the product during daytime, particularly for heavier rain rates. The RDT-CW product is able to identify around 60% of heavy ($>5\ mm{\cdot}hr^{-1}$) rainfall events with the fraction detected increasing with increasing rainfall rate. For both products, extrapolation forwards in time (up to 90 and 60 min, respectively) maintains useful skill in tropical Africa, motivating work to develop longer lead-time nowcasts. We conclude that widespread uptake of satellite nowcasting could provide new skilful weather predictions on short time-scales in much of tropical Africa.

KEYWORDS

convective rain, GPM, NWCSAF, precipitation, RDT, severe weather, SEVIRI, thunderstorms

1 | INTRODUCTION

As population growth and climate change increase exposure to weather hazards across much of the tropics, there is an urgent need to improve weather prediction and disaster early warning systems (U UNISDR, 2015; Kendon *et al*., 2019). Despite the continual improvements in numerical weather prediction (NWP) capabilities, extrapolation of precipitation observations still provides higher skill at the shortest time-scales (0–4 hr, Sun *et al*., 2014; 0–2 hr, Simonin *et al*., 2017). These extrapolation techniques could be of particular use in tropical Africa, where convective events can be long-lived and have severe impacts (Di Baldassarre *et al*., 2010; Webster, 2013) yet NWP skill remains poor, particularly at smaller spatial scales (Vogel *et al*., 2018; Kniffka *et al*., 2020) even for high-resolution convection-permitting models (Woodhams *et al*., 2018).

Rainfall radar observations provide accurate rainfall estimates at high temporal and spatial resolution and are usually the primary observation source for nowcasting (e.g., Browning and Collier, 1989; Wilson *et al*., 1998; Sun *et al*., 2014). While numerous studies have demonstrated the use of rainfall radar for research in Africa (e.g., de Coning *et al*., 2010; Lothon *et al*., 2011; Koffi *et al*., 2014), there are very few operational rainfall radar in tropical Africa. Consequently, nowcasting products must rely on satellite observations, with larger uncertainties. Such satellite observations are provided to African meteorological services through the Preparation for the Use of MeteoSat in Africa (PUMA) project. Yet nowcasting products are seldom if ever used by meteorological services in tropical Africa and it remains to be seen how skilful satellite-based nowcasting methods are in this region.

The European Organisation for the Exploitation of Meteorological Satellites (EUMETSAT) Nowcasting Satellite Applications Facility (NWCSAF) has developed a number of nowcasting products based on satellite measurements. These products were developed for use over Europe, with European imagery accessible through the NWCSAF website (http://www.nwcsaf.org/). However, the software is freely available to run in other regions such as tropical Africa. The Global Challenges Research Fund (GCRF) African Science for Weather Information and Forecasting Techniques (SWIFT; https://africanswift.org) project, which aims to develop sustained improvements in forecasting capabilities in tropical Africa, is investigating the use of NWCSAF products over tropical Africa in order to improve local nowcasting capabilities.

In April–May 2019, SWIFT held a 2 week, 24 hr·day^{-1} forecasting and nowcasting testbed in Nairobi, Kenya. This testbed introduced forecasters and researchers to new products in a quasi-operational, collaborative environment. The testbed was designed to test these new products with an aim toward eventually bringing them into operation for the many contributing operational centres, which included those from Kenya, Senegal, Ghana and Nigeria. One of the key products introduced in the testbed was the NWCSAF suite of products.

Feedback from this forecasting testbed highlighted the potential usefulness of these products in tropical Africa. NWCSAF products are being generated by the SWIFT team in the UK and shared publicly online (https://sci.ncas.ac.uk/swift/), and African groups are working to set up their own systems (with some success). Coincidentally, EUMETSAT has recently made some of the NWCSAF products available through EUMETCast-Africa for the entire earth disc centred at Null Island (0 ° N, 0 ° E); thus, NWCSAF products over the entire African continent are now available for any African forecasting centre to use.

Based on documented feedback from participants in this forecasting testbed, the two products that have been identified as most useful to forecasters are the convective rain rate (CRR) and rapidly developing thunderstorm convection warning (RDT-CW). The CRR aims to provide estimates of surface convective precipitation rates at the observation time; further extrapolated rain rates can be estimated every 15 min. While newer and more sophisticated rainfall algorithms than the CRR exist (e.g., Sorooshian *et al*., 2000; Lábó, 2012), it is worth highlighting again that the CRR software is available for free and runs in near real-time, which is crucial for nowcasting purposes. The RDT-CW product aims to identify, monitor, track and characterize convective events, thereby providing the forecaster with additional guidance on the occurrence and potential development of storms. Both these products are now distributed by NWCSAF and GCRF African SWIFT for the whole of Africa, although for NWCSAF this does not include extrapolated CRR estimates.

In order to use these newly available products appropriately, it is crucial that forecasters understand their errors and uncertainties. However, the products were developed for the mid-latitudes (i.e., Europe) and to our knowledge their evaluation is currently limited to Europe (Autones, 2016b; Marcos, 2016) and South Africa (de Coning *et al*., 2015; Gijben and de Coning, 2017). Consequently there is an urgent need for additional information on the performance of these products in tropical Africa, which is the primary aim of the present study.

The present study aims to provide an initial estimate of the performance of the CRR and RDT-CW products in tropical Africa, using global precipitation measurement (GPM) (Hou *et al*., 2014) Integrated Multisatellite Retrievals for GPM (IMERG) (Huffman *et al*., 2020) as "truth." The layout of the paper is as follows. In the next section we introduce the NWCSAF and IMERG datasets that are used the present study. In Section 3.1, we analyse

the CRR dataset and compare it to IMERG, first from a climatological perspective and then examining the skill of both the CRR retrieval and extrapolated CRR predictions. Subsequently, in Section 3.2, we consider the convective phase and severity attributes generated by the RDT-CW product and investigate how they relate to IMERG precipitation. Finally, we summarize the main findings of this analysis and discuss their implications for use of these nowcasting products in tropical Africa.

2 | METHODS

2.1 | Nowcasting products

Since March 2019, nowcasting products have been produced for three regions in tropical Africa (Figure 1) as part of the African SWIFT project. We call these regions Senegal (5.8 ° N–20.7 ° N, 23.9 ° W–7.5 ° W), Guinea coast (0.4 ° N–20.1 ° N, 12.0 ° W–17.6 ° E) and Kenya (6.4 ° S–8.5 ° N, 28.8 ° E–50.4 ° E). The products are generated using the 2016 version of the NWCSAF software and are based on spinning enhanced visible and infrared imager (SEVIRI) measurements combined with NWP data from the National Centers for Environmental Prediction Global Forecast System (GFS). Once generated, the products are viewable at https://sci.ncas.ac.uk/swift/. While the NWCSAF software can generate a wide range of products, in the present study we specifically focus on the two products that were identified by forecasters as most useful (i.e., CRR and RDT-CW). Both products are evaluated against microwave-based rainfall retrievals from the GPM IMERG product. The evaluation focuses on the period between March 1, 2019 (when these products were first

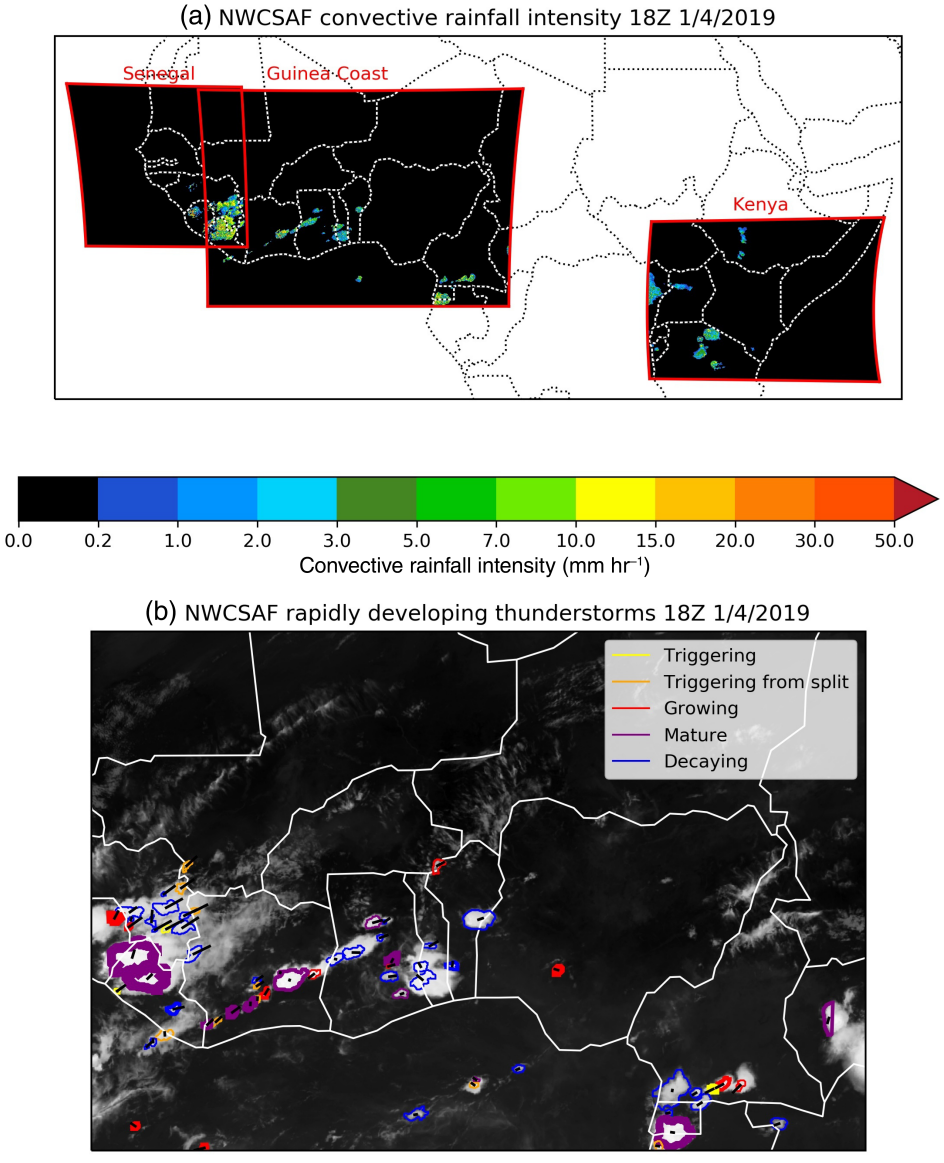

FIGURE 1 Example images for the two Nowcasting Satellite Applications Facility (NWCSAF) products considered in this paper. Both are for 1800 UTC on April 1, 2019. (a) The convective rain rate (CRR) for all three regions. (b) The rapidly developing thunderstorm convection warning (RDT-CW) product for the Guinea coast region. Here each closed contour denotes a RDT-CW cell. The colour of the contour denotes the development phase of the cell (see key), and the thickness of the contour denotes the severity of the cell, with "not defined" being the thinnest, low being the next thinnest and thicker contours corresponding to increasing severity. The black lines indicate the predicted location of the centre of gravity of the cell over the next 60 min. See the description of the RDT-CW product for further details regarding these storm attributes

made available through GCRF African SWIFT) and July 31, 2019 (based on availability of GPM IMERG final product data at the time of writing). In the interests of conciseness, the present study focuses specifically on the Guinea coast region. As the largest of the three regions, statistical sampling errors are smallest in the Guinea coast. The performance of the RDT and CRR products for the other two regions is very similar and the corresponding figures for these regions are available in Appendix S1.

2.1.1 | Convective rain rate

The CRR (Marcos and Rodriguez, 2016; Figure1a) is estimated using SEVIRI measurements in the 10.8 μm (infrared, IR), 6.2 μm (water vapour, WV) and (for solar zenith angles less than 80°) 0.6 μm (visible) channels. For night pixels (zenith > 80°), the CRR is determined as a function of the IR brightness temperature (BT) and the IR – WV BT difference, which predicts increasing CRR for lower IR BTs and smaller IR – WV BT absolute differences. For day pixels (zenith < 80°) the night time function (with different coefficients) is combined with an additional dependence on the normalised visible reflectance, which represents increasing CRR for more reflective clouds. These day–night differences are investigated as part of our evaluation of the CRR. The coefficients for both daytime and night time functions were obtained based on comparison with radar rainfall observations in Europe.

Once these initial CRR calculations are complete, a number of further corrections are applied. First, in order to eliminate stratiform precipitation, the CRR value obtained for any pixel from these functions is set to zero if all the pixels in a square of length 7 pixels centred on that pixel have a CRR lower than 3 $mm \cdot hr^{-1}$. Next, further corrections for humidity, evolution, gradient, parallax and orography are applied. The humidity correction increases (decreases) the CRR for pixels that correspond to a very moist (dry) atmosphere according to the NWP model. The evolution correction factor reduces the CRR for pixels that have warmer BTs than in the previous image. If the previous image is not available, the gradient correction factor is applied instead and reduces the CRR for pixels that do not correspond to a local minimum in BT. The parallax correction factor corrects for the location of cloudy pixels that are far from nadir, where the viewing geometry makes higher cloud appear to be further away. Finally, the orography correction factor increases (decreases) the CRR for pixels where the surface gradient following the 850 hPa NWP wind is increasing (decreasing). Note that since the humidity, evolution, gradient, parallax and orography corrections are applied after removal of "stratiform" precipitation it is possible for the final product to have large areas of non-zero CRR less than 3 $mm \cdot hr^{-1}$.

Extrapolated rain rates are calculated in 15 min increments by combining the analysed CRRs with the high resolution wind product, which estimates atmospheric motion vectors based on displacement of features between subsequent satellite images. For the CRR extrapolation, only high-level (above 400 hPa) winds are used. For the SWIFT products, to test the limits of the extrapolation capabilities, the extrapolation is run beyond the 60 min limit recommended by the NWCSAF developers to 90 min. Further details regarding the specifics of the CRR and extrapolation algorithms are available from Marcos and Rodriguez (2016) and ZAMG (2017), respectively.

2.1.2 | Rapidly developing thunderstorm convection warning

The RDT-CW product (Autones, 2016a) is developed by Meteo France. It uses an object oriented approach to add value to satellite imagery by characterizing the development of individual convective objects.

The first step of the RDT-CW algorithm is the identification of cloud pixels, based on the NWCSAF cloud type product. Within the cloud pixels, individual cloud towers (referred to as cells) are then identified based on the 10.8 μm BT and an adaptive BT threshold. Once the RDT-CW cells have been detected, they are tracked backwards in time based on overlap between cells in successive images. This generates a history and an estimate of the movement speed for each cell. The next step is the discrimination of convective cells, based on statistical models that use both NWP data and satellite measurements and are tuned against historical lightning data over Europe.

The RDT-CW algorithm determines a large number of attributes for each RDT-CW cell (e.g., cell area, cell advection, BT changes and difference in BT between channels), far too many for a forecaster to consider each attribute for each cell. To make the forecaster's task easier, many of these attributes are synthesized in new "phase of development" and "severity" attributes. The phase of development is determined from a combination of the cell's history, vertical extent, cooling rate, expansion rate, and overshooting top detection. The possible development phases are triggering, triggering from split, growing, mature and decaying. The severity attribute is based on one or more of the CRR, expansion rate or cooling rate exceeding specific thresholds or the presence of an overshooting top and is labelled as low, moderate,

high, very high or not defined. The not defined category corresponds to cells for which there are no overshooting tops and the other variables are unavailable. The identification of overshooting tops is primarily based on a pixel being 5 K colder than the tropopause, where the tropopause temperature is based on NWP data. When a pixel is only a little colder than the tropopause, additional criteria are applied, including visible reflectivity, BT differences between the 6.3 and 10.8 μm channels, and differences between a pixel and cell average temperature. Note that lightning data can also be used in the derivation of the phase and severity and results in an improved RDT-CW product (Gijben and de Coning, 2017). However, operational lightning data are not freely available in tropical Africa and thus cannot be used in the generation of NWCSAF products in this region. Further details on the RDT-CW algorithm are available from Autones (2016a).

There are numerous ways to visualize the RDT-CW product. For the African SWIFT project, the RDT-CW imagery is provided in the same format as the European imagery available through the NWCSAF website. An example is given in Figure 1(b). Each coloured contour denotes a distinct cell. The colour of the contour indicates the phase of development of the cell. The thickness of the contour indicates the severity of the cell. The straight black lines indicate the predicted location of the centre of gravity of the cell over the next 60 min.

As the RDT-CW algorithm tracks cells through time, missing data (e.g., due to problems retrieving the SEVIRI data) not only mean that the RDT-CW information for that point in time will be unavailable, but will affect subsequent times. In general, our analysis includes all RDT-CW data, irrespective of whether or not they may have been affected by missing data, the exception being for our analysis of changes in phase and severity between subsequent points in time, for which we exclude cells that are affected by missing data.

2.2 | Integrated multisatellite retrievals for global precipitation measurement

For evaluation of the NWCSAF products we use version 6 of the GPM (Hou *et al*., 2014) IMERG (Huffman *et al*., 2020). The IMERG dataset provides rainfall estimates every 30 min on a fixed latitude–longitude grid with a resolution of 0.1°.

For this study we use only the high quality measurements from this dataset, which are based solely on microwave observations. These are derived by taking microwave measurements from multiple imagers on multiple satellites (known as the GPM constellation), which are calibrated against coincident measurements from the microwave imager on the GPM core observatory. Tan *et al*. (2016) showed that these high quality IMERG estimates perform better than those based on other sources of information. Moreover, since they do not use SEVIRI measurements they are completely independent of the NWCSAF products. However, restricting the comparison to these high quality measurements means that we lose approximately two-thirds of the datapoints in the full GPM IMERG dataset, resulting in around 52 million comparable datapoints.

In order to provide some context for the NWCSAF CRR skill, climatological skill is derived from the GPM IMERG high quality data from previous years (i.e., 2000–2018). For each 0.1° and half hour window during the evaluation period, we take the climatological forecast as a random sample from a 7 day window centred on that forecast day from previous years' GPM IMERG high quality data at the exact same location and point in the diurnal cycle.

3 | RESULTS

3.1 | Evaluation of convective rain rate

For the purpose of these comparisons, the NWCSAF CRR is averaged to half hourly temporal and 0.1° spatial scales to match the IMERG temporal and spatial resolutions. Points for which either the high quality IMERG rainfall estimates or any of the CRR estimates are unavailable are excluded from the comparison.

Figure 2 compares the IMERG and CRR estimates from a climatological perspective. Rain is more frequent in the IMERG than in the CRR (Figure 2a), which is to be expected because the CRR algorithm removes "stratiform" rain and is unlikely to detect warm rain (i.e., produced by clouds with are entirely warmer than 0°C), particularly at night. Moreover, Figure 2a confirms that the increased detection of rain in IMERG is due to increased detection of low rain rates; the CRR detects rain rates higher than $\sim$3.5 mm·hr^{-1} more frequently than IMERG. IMERG detects rain more frequently during the night than during the day (defined here based on the use of short wave information in the NWCSAF CRR algorithm), but the distributions of non-zero rain rates are almost identical. The CRR also detects more rain during the night than during the day, but the CRR day and night time rainfall rate distributions are rather different: during the day, the CRR detects higher rain rates more frequently and lower rain rates less frequently. This difference can be explained by the use of the 0.6 μm channel in the CRR algorithm during the day, which facilitates

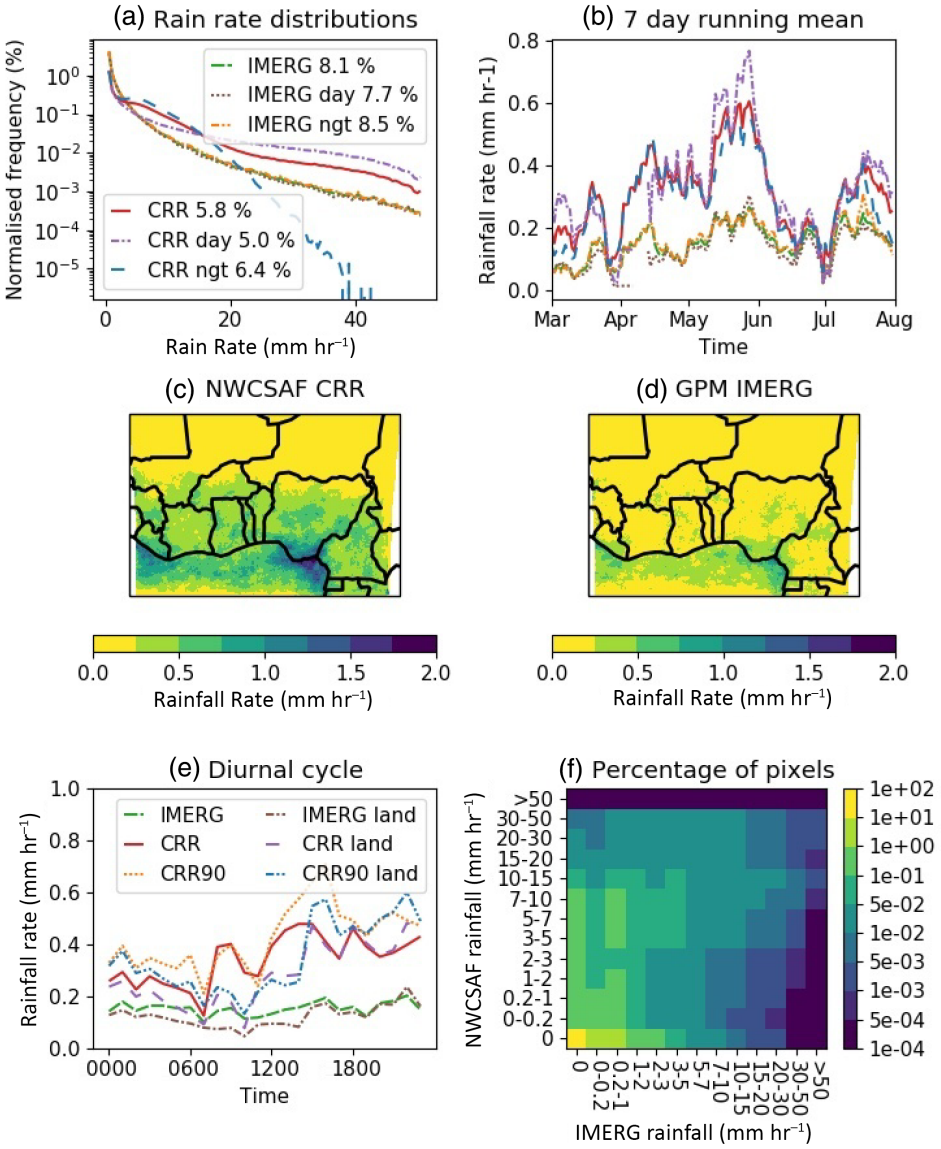

FIGURE 2 Comparison of global precipitation measurement (GPM) Integrated Multisatellite Retrievals for GPM (IMERG) high quality and Nowcasting Satellite Applications Facility (NWCSAF) convective rain rate (CRR) rainfall for March 1 to July 31, 2019 for the Guinea coast region. (a) The rainfall rate distributions, with the numbers in the key denoting the total frequency of rain detected. Note that the values are percentages of all points including non-raining. (b) Seven day running-mean domain mean rainfall. (c), (d) Mean geographical distributions of rainfall for the NWCSAF CRR and GPM IMERG products respectively. (e) The diurnal cycle of rainfall (hourly means), including the 90 min extrapolated CRR rainfall and with separate values for land pixels. (f) A one-to-one comparison of the two products

better identification of optically thick clouds which are more likely to be associated with higher rainfall rates. The increased frequency of higher rainfall rates estimated by the CRR algorithm relative to IMERG results in mean rainfall over the region (0.38 mm·hr^{-1}) that is more than twice that of IMERG (0.15 mm·hr^{-1}). The increased frequency of heavier rain rates during the day in the CRR retrieval leads to quite a large difference between the daytime and night time CRR mean rainfall (means of 0.43 and 0.35 mm·hr^{-1}, respectively).

The domain mean CRR is higher than that from IMERG throughout the period considered, but there is a notable reduction in the bias for June–July (Figure 2b). We hypothesize that this is due to a change in the domain mean diurnal cycle caused by the monsoon progression. As the monsoon progresses from the coast to further inland in June–July (e.g., Fink *et al*., 2017), mean rainfall over land increases (and the mean rainfall over ocean decreases). The domain mean diurnal cycle changes accordingly, with less of the total rainfall occurring during the day and more during the night (e.g., Figure 2e and Appendix S1). Since the CRR bias is larger during the day (Figure 2a), as daytime rainfall contributes less to total rainfall during June–July, the total rainfall bias compared to IMERG is reduced in this period.

The geographical distribution of rainfall is fairly similar in CRR and IMERG (Figure 2c and d, respectively). Both show their largest mean rainfall rates over the oceans, with regional maxima off the coasts of Liberia, Nigeria and Cameroon. IMERG rainfall is lower than the CRR throughout the region. Although the ratio and difference between the two estimates vary spatially, this appears to be simply sampling noise.

Over land, IMERG are consistent with the well-documented diurnal cycle of convection in the tropics

(Nesbitt and Zipser, 2003) with a peak in the evening and a minimum in the morning (Figure 2e). The amplitude of the diurnal cycle in IMERG is much smaller over the whole domain than it is over land, as although ocean accounts for only 18.6% of points in the comparison they account for 41.9% of the total IMERG precipitation (cf. Figure 2d).

The CRR mean rainfall is higher than IMERG throughout the day. The diurnal cycle for the CRR is dominated by a rapid increase around 1200 UTC, both over land and for all points. The amplitude of the diurnal cycle is larger for CRR than IMERG, but after normalizing to correct for the differences in mean rain rates (not shown) the amplitudes are reasonably similar. The mean 90 min forecast CRR values are higher than the mean instantaneous values throughout the diurnal cycle. This is true over both land and sea and all extrapolation times. The CRR mean values increase with increasing forecast range. Since the extrapolation simply advects existing precipitating systems, one might expect the extrapolated CRR values to lag behind the diurnal cycle of the instantaneous CRR; however, there is little evidence of this.

Comparing coincident rainfall estimates from the two products (Figure 2f), we see that, for IMERG rain rates <3 mm·hr^{-1}, the most common CRR category is no rain, which is consistent with the way "stratiform" rain is removed by the CRR algorithm. Similarly, for CRR rain rates <3 mm·hr^{-1} the most common IMERG category is no rain. For higher rain rates there does appear to be some skill, although CRR tends to overestimate the IMERG rain rate as might be expected based on their relative rain rate distributions.

Figure 3 evaluates the skill of the CRR rainfall estimates in terms of hit rates (the proportion of IMERG

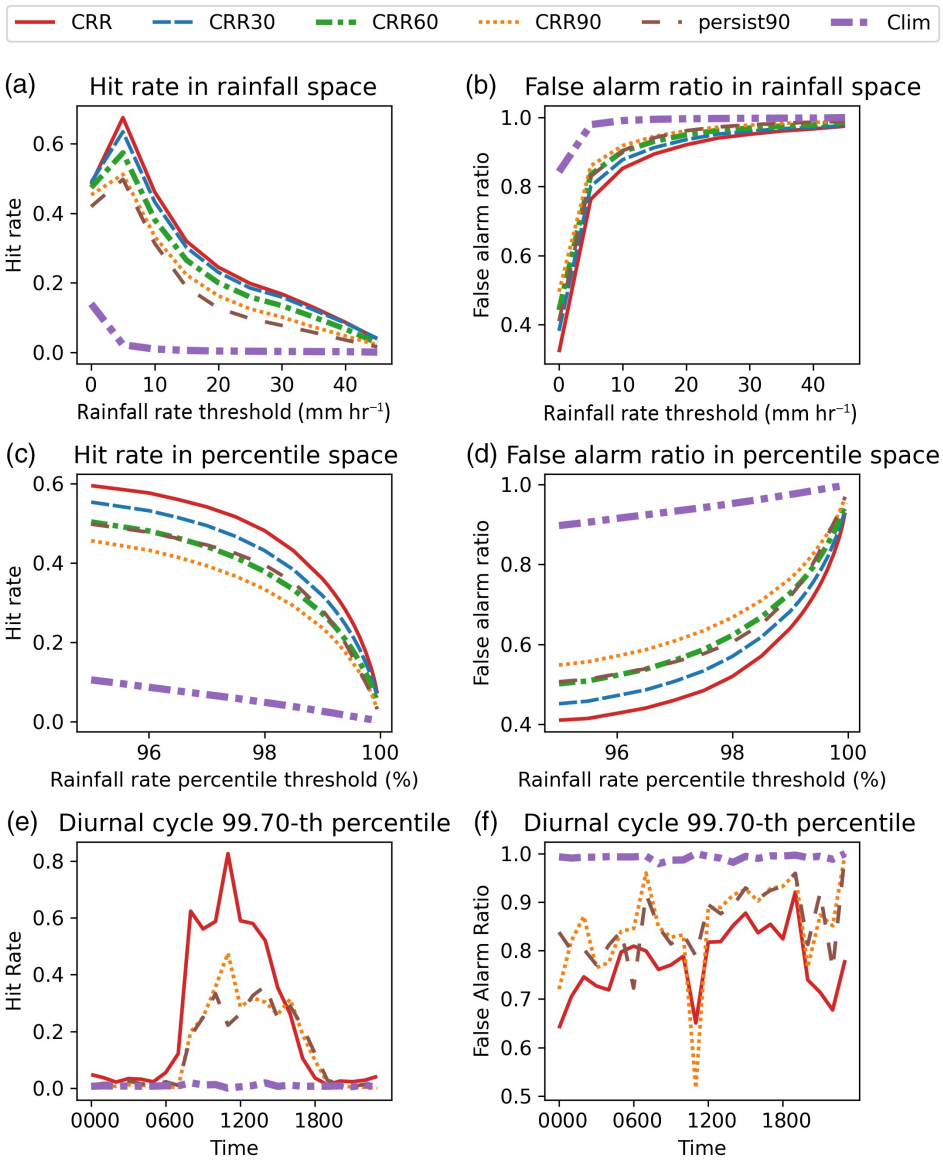

FIGURE 3 Hit rates and false alarm ratios for the Nowcasting Satellite Applications Facility (NWCSAF) convective rain rate (CRR) versus the global precipitation measurement (GPM) Integrated Multisatellite Retrievals for GPM (IMERG) high quality rainfall rates. CRR corresponds to the CRR retrieval; CRR30, CRR60 and CRR90 correspond to the 30, 60 and 90 min extrapolated CRR, respectively, as explained in Section 2.1.1. The persist90 lines correspond to 90 min persistence of the CRR retrieval and the Clim lines correspond to the IMERG climatology as described in Section 2.2. The left column (a), (c), (e) shows hit rates and the right column (b), (d), (f) shows false alarm ratios. The top row (a), (b) shows how the skill of the retrievals varies with differing rainfall rate thresholds. The second row (c), (d) shows how the skill of the retrievals varies for differing rainfall rate percentile thresholds. The bottom row (e), (f) shows how the skill varies with the diurnal cycle for the 99.7th rainfall rate percentile, which corresponds to 10.25 mm·hr^{-1} for the IMERG data, 19.52 mm·hr^{-1} for the CRR retrieval and 23.62 mm·hr^{-1} for the CRR 90 min forecast

rainfall events which are successfully forecast) and false alarm ratios (the proportion of rainfall event forecasts which are incorrect). Focusing first on the skill for the CRR retrieval (labelled CRR), Figure 3a shows a maximum hit rate for the 5 $mm \cdot hr^{-1}$ threshold, with the hit rate decreasing for higher thresholds. Nevertheless, the hit rate remains much larger than that for the climatology. The false alarm ratio is smallest for a threshold of 0 $mm \cdot hr^{-1}$ and increases with increasing rain rate, but remains smaller than that from the IMERG climatology.

Figure 3c,d shows how the hit rate and false alarm ratio change with different percentile thresholds. The impact of conducting the comparisons in percentile space can be largely explained by the biases in the CRR distribution. Since the CRR over-predicts rainfall rates greater than 3 $mm \cdot hr^{-1}$, which corresponds to approximately the 98.5th percentile for IMERG, both the hit rates and false alarm ratios are reduced above the 98.5th percentile threshold relative to those for a threshold of 3 $mm \cdot hr^{-1}$, whereas below these thresholds both the hit rate and false alarm ratio are increased. There is no obvious increase in overall skill simply by accounting for the difference in rainfall rate distributions between CRR and IMERG.

Figure 3e,f shows the hourly mean hit rate and false alarm ratio for the 99.7th percentile, which corresponds to approximately 10 $mm \cdot hr^{-1}$ for IMERG and 19 $mm \cdot hr^{-1}$ for the CRR retrieval. The hit rate is much larger during the day, while the false alarm ratio is also a little larger during the day. This is largely due to the increased frequency of CRR rainfall above this threshold during the day. It is also partly due to a real increase in the ability to detect heavy rainfall due to the use of short wave measurements: when separate 99.7th percentiles are applied to day and night, the daytime hit rate remains higher than that for the night (e.g., Figure S2, Appendix S1).

The skill for the extrapolated CRRs (CRR30, CRR60 and CRR90, as measured against IMERG) follows a very similar pattern to that for the CRR retrieval. The hit rate decreases and the false alarm ratio increases with increasing extrapolation time, but both remain much better than those calculated from the IMERG climatology (Figure 3a–d). The hourly mean hit rate for the 90 min extrapolated CRR appears to lag that for the CRR retrieval (Figure 3e,f) and as a result the 90 min extrapolated CRR has larger hit rates than the CRR retrieval around 1800 UTC. Again this is due to a combination of the over-prediction of heavy rain rates during the day and better identification of heavy precipitation due to the use of the short wave measurements.

Errors in the extrapolated CRR product can be caused by errors in the initial retrieval or errors in the extrapolation. Remarkably, persisting with the CRR retrieval for 90 min (labelled persist90 in Figure 3) provides more skill then the 90 min extrapolation, particularly in percentile space, which suggests that the extrapolation causes a reduction in skill. However, this is only true when evaluating against the IMERG rainfall as shown in Figure 3. If the extrapolation and persistence forecasts are evaluated against the CRR retrieval (Figure 4) then extrapolation results in higher hit rates and lower false alarm ratios than persistence, both in rainfall space and percentile space. Consequently, improvements to the CRR retrieval would also lead to significantly increased skill for the extrapolated rainfall estimates.

The improved skill of persistence relative to extrapolation when using IMERG as truth is thought to be caused by the increased bias (over-prediction of rainfall, cf. Figure 2e) for extrapolation combined with fortuitous cancellation of retrieval errors in the persistence estimate. In particular, based on analysis of individual images (not shown), CRR hits are often surrounded by broader areas of false alarms. This is because the algorithm struggles to separate precipitating and non-precipitating clouds and over-predicts rainfall occurrence (e.g., Figure 2a). As a precipitating system is advected, the precipitating part of the system will often coincide with areas which were previously non-precipitating cloud. Since these were erroneously identified as precipitation by the CRR algorithm, this will result in a hit for persistence.

3.2 | Interpretation of rapidly developing thunderstorm cells

Since the severity and phase information provided by RDT-CW are not well-defined measures that can be observed through other methods, the analysis of RDT-CW focuses on interpretation rather than evaluation. In particular, the aim is to understand how RDT-CW cells of different phase and severity relate to coincident and future heavy precipitation.

Figure 5 shows climatological properties of the RDT-CW cells. The cell phase (left hand column) appears to contain some useful information about the future lifecycle of the cell, with a higher proportion of decaying cells ceasing to exist on the subsequent time-step than the other phase types (Figure 5a). Moreover, the peak in area fraction (the total area of all cells of a given phase divided by the total area of the domain; Figure 5e) for growing cells precedes that for mature cells, which precedes that for decaying cells. Having said this, a large number of cells only persist for one time-step as indicated by the large number of cells with "none" as previous phase (Figure 5a). Most cells are also small.

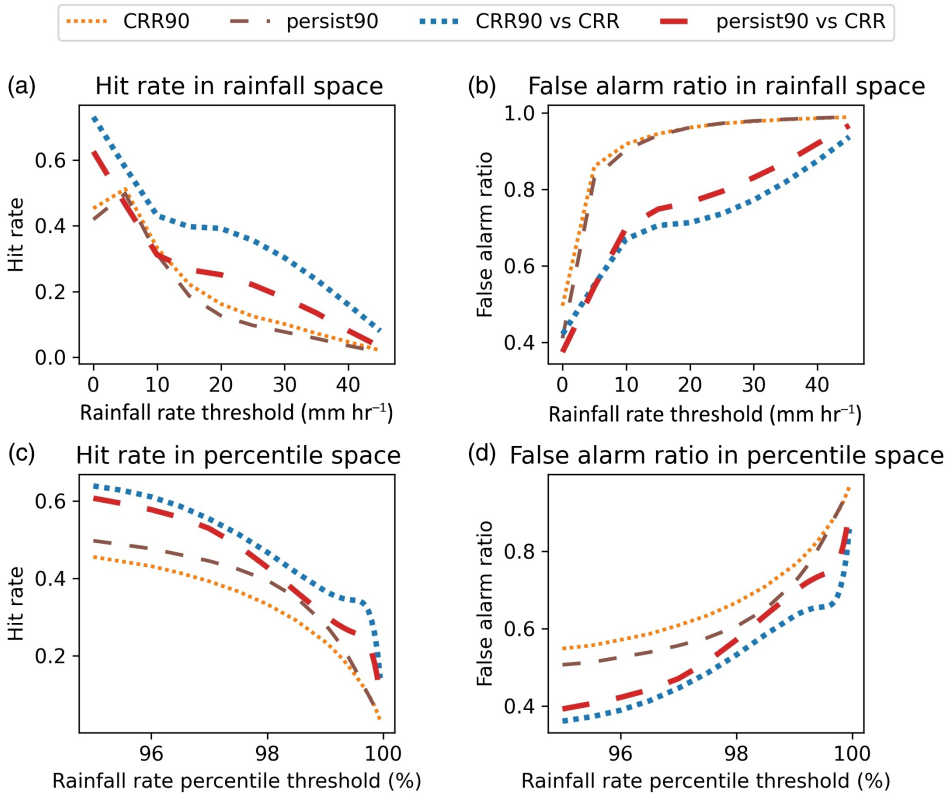

FIGURE 4 Comparison of 90 min forecasts of convective rain rates using either extrapolation or persistence, with the "truth" being either global precipitation measurement (GPM) Integrated Multisatellite Retrievals for GPM (IMERG) or the instantaneous convective rain rate (CRR) retrieval. The left column (a), (c) shows hit rates and the right column (b), (d) shows false alarm ratios. The top row (a), (b) shows how the skill of the retrievals varies with differing rainfall rate thresholds. The bottom row (c), (d) shows how the skill of the retrievals varies for differing rainfall rate percentile thresholds

This prevalence of small short-lived cells is consistent with previous studies of the convective lifecycle in tropical Africa (e.g., Taylor, 2017; Crook *et al*., 2019). Nevertheless, user feedback within the African SWIFT project suggests that the number of small short-lived cells produced by the RDT-CW product can be rather overwhelming for users of the product.

The cell severity appears to be less useful for understanding the likely future of the cell, not least because the most common severity type is "not defined" (Figure 5b). Interestingly, the size distributions for high and very high severity cells are bi-modal. In addition to the maximum occurrence for cells with an area between 100 and 1,000 km^2 common to all severities, high and very high severity cells show a second local maximum for cells with an area of ~10,000 km^2. This seems likely to be a consequence of the way the severity is determined, as described in Section 3, as larger cells have more pixels giving them a greater chance to meet one of the criteria that correspond to higher severity. While the severity may not be that useful for predicting the future of a cell, the diurnal cycle of cell severity area fractions (Figure 5f) suggests that the severity of the cell may be useful for identifying the amount of precipitation, with the diurnal phase for high and very high severity cells matching that for precipitation, whereas the maximum occurrence of low severity cells precedes this.

Figure 6 shows how RDT-CW cells relate to IMERG rain rates. Since the RDT-CW cells and their phases and strengths are discrete variables that cannot be meaningfully averaged, this analysis is based on identifying whether any RDT-CW cells overlap with each IMERG pixel. In many cases, an IMERG pixel may coincide with multiple RDT-CW cells. If these cells have differing values for the phase or strength then they are included in a "multiple" cell category, and the fractional occurrence of each phase or strength is used to accumulate the frequency of different phase and strength values within this multiple cell category.

The RDT software may change some of the attributes of a cell as it is extrapolated forwards in time based on the observed trends in these attributes. However, since the imagery provided only indicates the current phase and strength, we use these original values for the evaluation of the extrapolated cells.

Figure 6a shows that more than 60% of heavy rainfall rates (i.e., exceeding 5 $mm \cdot hr^{-1}$) coincide with an RDT-CW cell, with this fraction increasing as the rainfall rate increases. The most common phase for these cells is mature and the fraction that are labelled as mature also increases with increasing rain rate. Similarly, the most common severity for heavy rain rates is very high (Figure 6b) and the fraction that are identified as very high severity also increase with increasing rain rate. For the 60 min extrapolated RDT-CW cells, we see similar behaviour

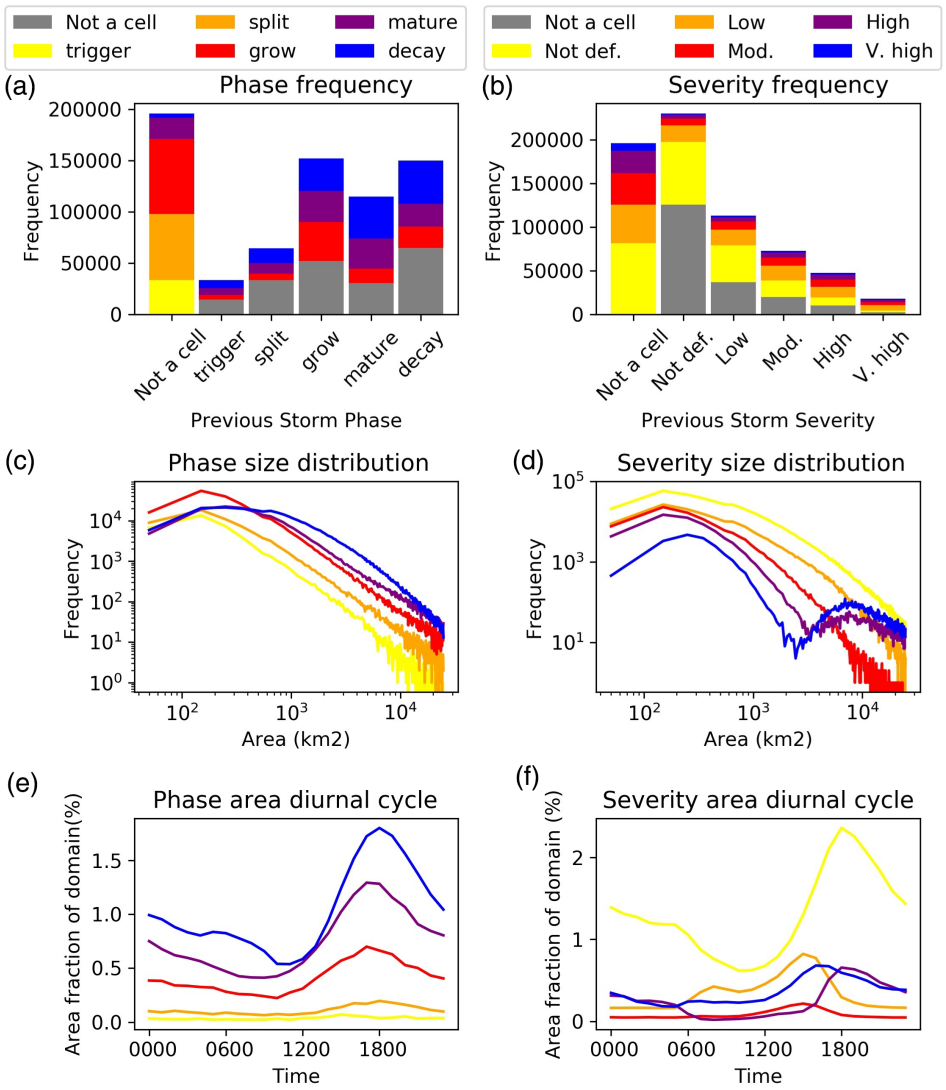

FIGURE 5 Climatology of the occurrence of rapidly developing thunderstorm (RDT) cells of different phase and severity, from March 1, 2019 to July 31, 2019. The left column is for lifecycle phase and the right column is for severity. The upper row (a), (b) shows the number of cells of each phase/severity and their phase and severity in the subsequent image. For these two panels, cells that were affected by missing data were excluded. The middle row (c), (d) shows the size distribution of cells of each phase/severity. The bottom row (e), (f) shows the hourly area fraction of the domain for storms of each phase/severity. The legends are representative for their respective columns

(Figure 6c,d), but a larger fraction of the rainfall events are missed. Nevertheless, more than half the heavy rain rates coincide with 60 min extrapolated RDT-CW cells.

Considering the diurnal cycle of rainfall (Figure 6e,f), there is a slight increase in the fraction of heavy rainfall events that coincide with RDT-CW cells between 1730 and 0030, which coincide with an increase in the number that are identified as high severity. This contrasts with the CRR product which produces fewer heavy rain events during the night.

4 | SUMMARY AND OUTLOOK

There is an urgent need to improve weather predictions across time-scales in Africa to increase resilience to extreme weather, including extreme rainfall, which is expected to increase with climate change (Kendon *et al.*, 2019). We have investigated the properties and ability to detect rainfall in tropical Africa for two satellite-based nowcasting products, the rapidly developing thunderstorm convection warning (RDT-CW) and the convective rain rate (CRR). We have focused on a broad region centred on the Guinea coast, but analysis over other regions in tropical Africa shows similar results (see Appendix S1), which is encouraging for possible future widespread uptake of these products across tropical Africa. Both products show useful skill in identifying heavy rainfall events both at the retrieval time and when extrapolated forward in time. This is consistent with subjective conclusions based on trial use of these products by forecasters within the African Science for Weather Information and Forecasting Techniques (SWIFT) project.

While both products have useful skill, they also have a number of weaknesses. One of the main problems we identified with the CRR product is the difference between day and night retrievals. Day and night rainfall rate distributions are quite different, with heavy rainfall rates

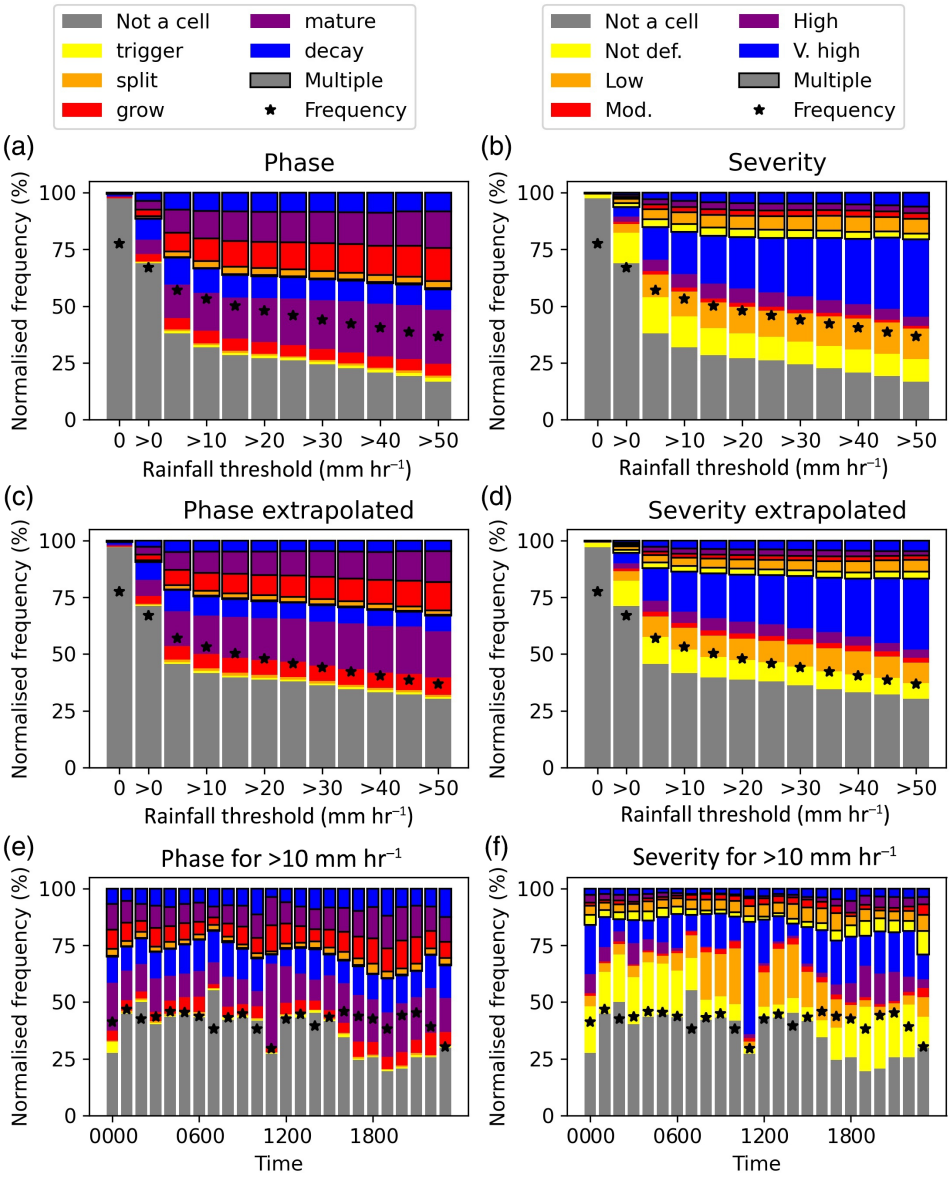

FIGURE 6 Overlap occurrence of rapidly developing thunderstorm convection warning (RDT-CW) cells of different phases (left column) and severity (right column) with global precipitation measurement (GPM) Integrated Multisatellite Retrievals for GPM (IMERG) high quality pixels exceeding given rainfall thresholds. The first row (a), (b) shows the occurrence of RDT-CW cells for different IMERG rain rate thresholds. The second row (c), (d) shows the occurrence of 60 min extrapolated RDT-CW cells for different IMERG rain rate thresholds. The third row (e), (f) shows the diurnal cycle of occurrence of RDT-CW cells with IMERG pixels that have rain rates greater than 10 mm·hr^{-1}. The asterisk on each of the bars denotes the frequency of occurrence of the event in the IMERG data; the location on the *y*-axis for this asterisk corresponds to 10 times the decimal logarithm of the frequency. The keys are representative for their respective columns

being more likely during the day. While the night time retrieval could be applied during the day, this would result in a reduction in skill, as the daytime retrieval has higher hit rates, even after differences in the rainfall rate distributions are considered. Ideally these issues would be addressed by retuning the algorithm for tropical Africa, yet a lack of high quality observations makes this difficult. As things stand, given the large differences between day and night retrievals, the CRR imagery should indicate which algorithm has been applied.

Fundamentally the skill of any rainfall estimate based on geostationary satellite observations will be limited by the fact that the measurements are not directly sensitive to rainfall. Nevertheless, we have demonstrated that the CRR is skilful in tropical Africa. There are a number of alternative products that derive rainfall estimates from geostationary satellite data at the high temporal resolutions required for nowcasting (e.g., precipitation estimation from remotely sensed information using artificial neural networks, PERSIANN; Sorooshian *et al.*, 2000), which may be able to achieve even higher skill. Of particular interest are techniques that use microwave observations to perform continual local "calibration" of the geostationary satellite precipitation retrieval (e.g., Hong *et al.*, 2005). These techniques address the issue of tuning rainfall estimates for tropical Africa. Moreover, nowcasting rainfall products using these techniques already exist through the EUMETSAT Support to Operational Hydrology and Water Management Satellite Applications Facility (H-SAF). While it is beyond the scope of the African SWIFT project, the use of other rainfall products for nowcasting in tropical Africa is certainly worth investigating.

Since the RDT-CW algorithm uses the CRR product, improvements to the CRR should feed into improvements in RDT-CW. Feedback within the African SWIFT project suggests that the large number of small short duration cells identified by the RDT-CW product can be rather overwhelming for forecasters. It would be useful to consolidate some of this information, either by retuning the product for the tropics to produce fewer small short-lived cells, or by changing the way the product is displayed.

Since both products maintain skill at the 90 min limit of the extrapolation times tested here, it would also be valuable to extrapolate both further forward in time. In this context it would also be worth considering how skill varies with spatial scales, particularly for the extrapolated products, which may suffer from the well-known (Mass *et al*., 2002) "double penalty" problem, where a small error in the location or timing of an event results in both a miss and a false alarm and thus can result in lower apparent skill then failing to forecast the event at all.

Many leading weather forecasting centres now have nowcasting systems that seamlessly blend extrapolated observations with numerical weather prediction (NWP) output, with an increasing dependence on the latter for longer lead times (Sun *et al*., 2014; Kotsuki *et al*., 2019; Nerini *et al*., 2019). A direct comparison between NWP and nowcasting skill for tropical Africa would be useful not only in this context but also for forecasters who need to try to combine both these sources of information optimally.

This study has demonstrated that the Nowcasting Satellite Applications Facility (NWCSAF) products can provide skilful weather predictions on short time-scales for tropical Africa. As such, widespread uptake of these nowcasting products could provide improved short-range forecasts in tropical Africa. The NWCSAF products will continue to be investigated and developed within the Global Challenges Research Fund African SWIFT project. In particular, future work will aim to evaluate both retrieved and extrapolated data from both the CRR and RDT-CW products against rain gauge data, investigate how well the RDT-CW cells relate to lightning observations, and provide longer lead-time predictions.

ACKNOWLEDGEMENTS

We would like to thank the Nowcasting Satellite Applications Facility for provision of the nowcasting software, the EUMETSAT EUMETcast Africa service for provision of satellite data, and the Chilbolton Observatory for assistance with receiver siting and maintenance. Thanks also to the participants in the April–May 2019 African SWIFT testbed for feedback on the nowcasting products, Dan Walker from the National Centre for Atmospheric Science for his work on the SWIFT nowcasting catalogue, and staff from the South African Weather Service for their valuable insights into the setup and use of the NWCSAF products. We are grateful to two anonymous reviewers for their considered and insightful comments and suggestions. NWCSAF software used to generate the CRR and RDT-CW products is freely available to registered users and can be downloaded from the NWCSAF website (http://www.nwcsaf.org). SEVIRI data input to the NWCSAF software is available from the EUMETSAT Earth Observation Portal (https://eoportal.eumetsat.int). NCEP GFS NWP data, which are also used as input to the NWCSAF software in the present study, are available through the National Centers for Environmental Information website (https://www.ncdc.noaa.gov/data-access/model-data/model-datasets/global-forcast-system-gfs). IMERG data are available from the NASA Goddard Earth Sciences Data and Information Services Centre (GES DISC; https://disc.gsfc.nasa.gov/datasets/GPM_3IMERGHH_06/summary). Python code used for the analysis described in this paper is freely available on GitHub (https://github.com/PeterGHill/NWCSAF-Eval). This work was supported by UK Research and Innovation as part of the Global Challenges Research Fund, African SWIFT programme, grant number NE/P021077/1. Marsham was also supported by the National Centre for Atmospheric Science via the NERC/GCRF programme ACREW: Atmospheric Hazard in Developing Countries: Risk Assessment and Early Warning.

ORCID

Peter G. Hill https://orcid.org/0000-0002-9745-2120

REFERENCES

Autones, F. (2016a) Algorithm theoretical basis document for convection products. Online. http://www.nwcsaf.org/AemetWebContents/ScientificDocumentation/Documentation/GEO/v2016/NWC-CDOP2-GEO-MFT-SCI-ATBD-Convection_v1.1.pdf. Accessed 23 September 2020.

Autones, F. (2016b) Validation report of the Convection Product Processors of the NWC/GEO. Online. http://www.nwcsaf.org/AemetWebContents/ScientificDocumentation/Documentation/GEO/v2016/NWC-CDOP2-GEO-MFT-SCI-VR_v1.0.pdf.

Browning, K.A. and Collier, C.G. (1989) Nowcasting of precipitation systems. *Reviews of Geophysics*, 27(3), 345.

Crook, J., Klein, C., Folwell, S., Taylor, C.M., Parker, D.J., Stratton, R. and Stein, T. (2019) Assessment of the representation of west African storm lifecycles in convection-permitting simulations. *Earth and Space Science*, 6, 818–835.

de Coning, E., Gijben, M., Maseko, B. and van Hemert, L. (2015) Using satellite data to identify and track intense thunderstorms in south and southern Africa. *South African Journal of Science*, 111(7/8), 51–59.

de Coning, E., Koenig, M. and Olivier, J. (2010) The combined instability index: a new very-short range convection forecasting technique for southern Africa. *Meteorological Applications*, 18 (4), 421–439.

Di Baldassarre, G., Montanari, A., Lins, H., Koutsoyiannis, D., Brandimarte, L. and Blöschl, G. (2010) Flood fatalities in Africa: from diagnosis to mitigation. *Geophysical Research Letters*, 37(22), L22402. https://doi.org/10.1029/2010GL045467.

Fink, A.H., Engel, T., Ermert, V., van der Linden, R., Schneidewind, M., Redl, R., Ernest Afiesimama, W.M., Thiaw, C. Y., Evans, M. and Janicot, S. (2017) Mean climate and seasonal cycle. *Meteorology of tropical West Africa: the Forecasters' Handbook*. Chichester, UK: John Wiley & Sons Ltd., 1–39. https://onlinelibrary.wiley.com/doi/10.1002/9781118391297.ch1.

Gijben, M. and de Coning, E. (2017) Using satellite and lightning data to track rapidly developing thunderstorms in data sparse regions. *Atmosphere*, 8(12), 67.

Hong, Y., Hsu, K.-L., Sorooshian, S. and Gao, X. (2005) Improved representation of diurnal variability of rainfall retrieved from the tropical rainfall measurement mission microwave imager adjusted precipitation estimation from remotely sensed information using artificial neural networks (PERSIANN) system. *Journal of Geophysical Research*, 110, D06102. https://doi.org/10.1029/2004JD005301.

Hou, A.Y., Kakar, R.K., Neeck, S., Azarbarzin, A.A., Kummerow, C. D., Kojima, M., Oki, R., Nakamura, K. and Iguchi, T. (2014) The global precipitation measurement mission. *Bulletin of the American Meteorological Society*, 95(5), 701–722.

Huffman, G.J., Bolvin, D.T., Braithwaite, D., Hsu, K., Joyce, R., Kidd, C., Nelkin, E.J., Sorooshian, S., Tan, J. and Xie, P. (2020) NASA global precipitation measurement (GPM) integrated multi-satellite retrievals for GPM (IMERG) Algorithm Theoretical Basis Document, Version 06. In: *Online*. https://gpm.nasa.gov/sites/default/files/2020-05/IMERG_ATBD_V06.3.pdf. Accessed 23 September 2020.

Kendon, E.J., Stratton, R.A., Tucker, S., Marsham, J.H., Berthou, S., Rowell, D.P. and Senior, C.A. (2019) Enhanced future changes in wet and dry extremes over Africa at convection-permitting scale. *Nature Communications*, 10, 1794. https://doi.org/10.1038/s41467-019-09776-9.

Kniffka, A., Knippertz, P., Fink, A.H., Benedetti, A., Brooks, M.E., Hill, P.G., Maranan, M., Pante, G. and Vogel, B. (2020) An evaluation of operational and research weather forecasts for southern West Africa using observations from the DACCIWA field campaign in June–July 2016. *Quarterly Journal of the Royal Meteorological Society*, 146, 1121–1148.

Koffi, A.K., Gosset, M., Zahiri, E.-P., Ochou, A.D., Kacou, M., Cazenave, F. and Assamoi, P. (2014) Evaluation of X-band polarimetric radar estimation of rainfall and rain drop size distribution parameters in West Africa. *Atmospheric Research*, 143, 438–461.

Kotsuki, S., Kurosawa, K., Otsuka, S., Terasaki, K. and Miyoshi, T. (2019) Global precipitation forecasts by merging extrapolation-based nowcast and numerical weather prediction with locally optimized weights. *Weather and Forecasting*, 34(3), 701–714.

Lábó, E. (2012) Validation studies of precipitation estimates from different satellite sensors over Hungary—analysis of new satellite-derived rain rate products for hydrological purposes. *Journal of Hydrology*, 468-469, 173–187.

Lothon, M., Campistron, B., Chong, M., Couvreux, F., Guichard, F., Rio, C. and Williams, E. (2011) Life cycle of a mesoscale circular gust front observed by a C-band Doppler radar in West Africa. *Monthly Weather Review*, 139(5), 1370–1388.

Marcos, C. (2016) Scientific and validation report for the precipitation product processors of the NWC/GEO. http://www.nwcsaf.org/AemetWebContents/ScientificDocumentation/Documentation/GEO/v2016/NWC-CDOP2-GEO-AEMET-SCI-VR-Precipitation_v1.0.pdf. Accessed 23 September 2020.

Marcos, C. and Rodriguez, A. (2016) Algorithm theoretical basis document for the Precipitation Product Processors of the NWC/GEO. Online. http://www.nwcsaf.org/AemetWebContents/ScientificDocumentation/Documentation/GEO/v2016/NWC-CDOP2-GEO-AEMET-SCI-ATBD-Precipitation_v1.1.pdf.

Mass, C.F., Ovens, D., Westrick, K. and Colle, B.A. (2002) Does increasing horizontal resolution produce more skillful forecasts? *Bulletin of the American Meteorological Society*, 83(3), 407–430.

Nerini, D., Foresti, L., Leuenberger, D., Robert, S. and Germann, U. (2019) A reduced-space ensemble Kalman filter approach for flow-dependent integration of radar extrapolation nowcasts and NWP precipitation ensembles. *Monthly Weather Review*, 147(3), 987–1006.

Nesbitt, S.W. and Zipser, E.J. (2003) The diurnal cycle of rainfall and convective intensity according to three years of TRMM measurements. *Journal of Climate*, 16(10), 1456–1475.

Simonin, D., Pierce, C., Roberts, N., Ballard, S.P. and Li, Z. (2017) Performance of Met Office hourly cycling NWP-based nowcasting for precipitation forecasts. *Quarterly Journal of the Royal Meteorological Society*, 143(708), 2862–2873.

Sorooshian, S., Hsu, K.-L., Gao, X., Gupta, H.V., Imam, B. and Braithwaite, D. (2000) Evaluation of PERSIANN system satellite-based estimates of tropical rainfall. *Bulletin of the American Meteorological Society*, 81(9), 2035–2046.

Sun, J., Xue, M., Wilson, J.W., Zawadzki, I., Ballard, S.P., Onvlee-Hooimeyer, J., Joe, P., Barker, D.M., Li, P.-W., Golding, B., Xu, M. and Pinto, J. (2014) Use of NWP for nowcasting convective precipitation: recent progress and challenges. *Bulletin of the American Meteorological Society*, 95(3), 409–426.

Tan, J., Petersen, W.A. and Tokay, A. (2016) A novel approach to identify sources of errors in IMERG for GPM ground validation. *Journal of Hydrometeorology*, 17(9), 2477–2491.

Taylor, S. (2017) High time-resolution observations of convective cloud lifecycles. Online. https://ora.ox.ac.uk/objects/uuid:96a5d923-e5eb-4d81-a87c-d8718fb654b4/download_file?file_format=pdf&safe_filename=thesis_ora_dissemination.pdf&type_of_work=Thesis. Accessed on Fri, March 20, 2020.

U UNISDR. (2015) Sendai framework for disaster risk reduction 2015–2030. In: *Proceedings of the 3rd United Nations World Conference on DRR, Sendai, Japan*, pp. 14–18. https://www.unisdr.org/files/45069_proceedingsthirdunitednationsworldc.pdf. Accessed 23 September 2020.

Vogel, P., Knippertz, P., Fink, A.H., Schlueter, A. and Gneiting, T. (2018) Skill of global raw and postprocessed ensemble predictions of rainfall over northern tropical Africa. *Weather and Forecasting*, 33(2), 369–388.

Webster, P.J. (2013) Improve weather forecasts for the developing world. *Nature*, 493(7430), 17–19.

Wilson, J.W., Crook, N.A., Mueller, C.K., Sun, J. and Dixon, M. (1998) Nowcasting thunderstorms: a status report. *Bulletin of the American Meteorological Society*, 79(10), 2079–2099.

Woodhams, B.J., Birch, C.E., Marsham, J.H., Bain, C.L., Roberts, N. M. and Boyd, D.F.A. (2018) What is the added value of a convection-permitting model for forecasting extreme rainfall over tropical East Africa? *Monthly Weather Review*, 146(9), 2757–2780.

ZAMG (2017) Algorithm theoretical basis document for the extrapolated imageryprocessor of the NWC/GEO. Online. http://www.nwcsaf.org/AemetWebContents/ScientificDocumentation/Documentation/GEO/v2016/NWC-CDOP2-GEO-ZAMG-SCI-ATBD-EXIM_v1.1.pdf. Accessed 23 September 2020.

SUPPORTING INFORMATION

Additional supporting information may be found online in the Supporting Information section at the end of this article.

How to cite this article: Hill PG, Stein THM, Roberts AJ, Fletcher JK, Marsham JH, Groves J. How skilful are Nowcasting Satellite Applications Facility products for tropical Africa? *Meteorol Appl*. 2020;27:e1966. https://doi.org/10.1002/met.1966